Surface & Coatings Technology 401 (2020) 126235

Contents lists available at ScienceDirect

Surface & Coatings Technology

journal homepage: www.elsevier.com/locate/surfcoat

Tailoring CrN_x stoichiometry and functionality by means of reactive HiPIMS

J.C. Sánchez-López[a,*], A. Caro[a], G. Alcalá[b], T.C. Rojas[a]

[a] Instituto de Ciencia de Materiales de Sevilla (CSIC-Univ. Sevilla), Avda. Américo Vespucio 49, 41092 Sevilla, Spain
[b] Department of Chemical and Materials Engineering, Faculty of Chemistry, Complutense University of Madrid, Ciudad Universitaria s/n, 28040 Madrid, Spain

ARTICLE INFO

Keywords:
HiPIMS
Duty cycle
Pulse
Oxidation resistance
Hardness
Bias

ABSTRACT

This work presents a complete study of the influence of HiPIMS pulse characteristics on the microstructure, chemical composition, mechanical and oxidation resistance properties of CrN thin films. The investigated parameters were frequency and pulse length at two different nitrogen fluxes, maintaining constant the duty cycle conditions (2%). The effect of a negative bias of 100 V was investigated in a particular case. By changing the synthesis conditions, it was possible to tailor the N/Cr ratio and thus to control the CrN_x stoichiometry from x = 0.63 to 1.10. The selection of longer pulses (shorter frequencies) generates more disordered structures with lower N/Cr ratios. This is reflected in higher hardness and elastic modulus values on despite of a lower oxidation resistance due to existence of larger concentration of N vacancies. The best oxidation resistance is obtained at the highest peak current combined with additional ion bombardment provided by substrate biasing. The present results open the possibilities of modifying chemical composition and engineering surfaces by changing exclusively the pulse conditions in HiPIMS deposition processes.

1. Introduction

The high power impulse magnetron sputtering (HiPIMS) technology has attracted considerable attention from researchers and industries in the last decades. High peak current (> 1 A/cm^2), peak power densities (0.1–3 kW/cm^2), plasma densities (10^{19} m^{-3}) and ionization rates (> 40%), can be achieved improving film density and functionality by the application of short pulses (typically 50–500 μs) at low frequencies (< 1 kHz). This technique enables homogeneous thickness on complex-shaped tools with good adhesion even on surfaces non-parallel to the target. The incorporation of macroparticles is also significantly reduced in comparison to cathodic arc-physical vapor deposition (PVD) technology, decreasing porosity and reinforcing film density. These characteristics have positioned HiPIMS as a promising technology for hard coatings on cutting and forming tools [1–6].

Transition metal nitrides have been extensively deposited by PVD techniques for multiple functional applications as hard protective coatings with excellent adhesion to steel [7,8]. Control of the metal nitrides stoichiometry is a crucial issue in thin film deposition [9]. The changes on the metal/nitrogen ratio determine phase composition, crystal structure, film morphology, thermal stability, and many other structural and chemical properties affecting the final performance (optical, electrical, mechanical, oxidation resistance, etc.) [10–13]. In certain applications, a graded chemical composition (gradient or multilayer architecture) is searched deliberately in order to achieve a good adhesion on the substrate, and a progressive adaptation to the desired functionality. Gradient interlayers are usually employed in DLC deposition procedures to obtain adherent films on metallic substrates with optimum tribomechanical performance and reduced stress [14,15]. Other examples of applications of metal nitrides are diffusion barrier layers, infrared or decorative coatings, where the precise control of stoichiometry results primordial to tailor their practical performance. Particularly, Cr(Al)N films have been perhaps one of the most studied systems due to their high hardness, corrosion-resistant and anti-wear properties, with a high demand in many industrial applications like molding, forging, machining and plastic processing [6,16–24]. Many established PVD methods have been employed for the preparation of these hard transition metal nitride coatings, like vacuum-arc [25], pulsed laser deposition [26], DC-magnetron sputtering [12,17,18], pulsed-DC (10–350 kHz) [27], and more recently, HiPIMS and modulated pulsed power-MPP (< 1 kHz) [5,6,16,28–30].

Previous works have shown the possibilities that HiPIMS offers to influence chemical composition, microstructure, phases and mechanical properties by changing the pulse parameters [6,22,30–34]. Denser and finer grain morphologies are obtained by shortening the pulse length and therefore, increasing the maximum peak current a [6,28,31]. Besides the pulse characteristics, an important although less studied parameter is the chosen duty cycle (η). Many of the previous

* Corresponding author.
E-mail address: jcslopez@icmse.csic.es (J.C. Sánchez-López).

https://doi.org/10.1016/j.surfcoat.2020.126235
Received 16 December 2019; Received in revised form 12 July 2020; Accepted 26 July 2020
Available online 27 July 2020

literature data studied the influence of pulse duration or frequencies on plasma discharges and film properties without keeping constant this important parameter. The chosen pulse on/off time configuration has been demonstrated to influence noteworthy the deposition rate [34,35] and the coating properties [29,34,36]. Hsiao et al. showed that peak power density increased linearly as the duty cycle decreased from 5 to 2% at constant frequency [29]. Both parameters have a strong influence on the microstructure evolution from coarse to fine columnar.

In this paper, we report the potentialities of HiPIMS working in reactive mode to tune the metal/nitrogen ratio in CrN_x films maintaining constant duty cycle and average target power. The pulse length (frequency) values were varied at fixed $\eta = 2\%$ to deposit different films at two N_2/Ar ratios. The structural and chemical characterization of the films allows the establishment of a correlation between synthesis conditions, achieved stoichiometry and functional properties. The obtained results are compared with those obtained by conventional direct current (DC) magnetron sputtering and one biased-HiPIMS sample at 100 V. These results are very useful for engineering surfaces and multilayered coatings in reactive HiPIMS processes by simply changing the pulse characteristics at fixed gas flows.

2. Experimental

CrN coatings were prepared by HiPIMS using a Cr target (99.95% purity, 3.2 mm thick) connected to a HiPIMS source from Solvix® (HIP3), working at a nominal power of 300 W. A circular 2-inch balanced magnetron was used with a racetrack surface representing about the 30% of the total area. The total area 20.27 cm^2 was used for calculation of the power densities. The pumping system allows a base pressure of $\sim 1 \times 10^{-4}$ Pa in the synthesis chamber. The nitrogen and argon fluxes used for the deposition are summarized in Table 1 together with the pulse characteristics. Two sets of samples were prepared by changing the nitrogen flux (2 and 4 sccm respectively) at a constant argon flow of 20 sccm and a working total pressure of ≈ 0.9 Pa. These conditions correspond to the metallic-transition regime according to preliminary studies that revealed that compound mode appeared between 5 and 11 sccm for this chamber. Three different pulse conditions were used for each one of these sets, with pulse lengths ranging from 20 to 100 μs and frequencies ranging from 200 to 1000 Hz, as described in Table 1. The selected pulse parameters were chosen in order to keep constant the duty cycle ($\eta = 2\%$). During film deposition, the substrates were moving in a one-fold rotation holder at 35 RPM placed at 10 cm from the target. An additional coating was prepared at 4 sccm of N_2 without pulses using the same effective average power for comparison purposes (non-pulsed DC). The HiPIMS conditions used in coating D were also employed in combination with a negative polarization to the substrate (bias) of 100 V using a DC-pulsed source working at 250 kHz and $\eta = 87.6\%$. The temperature of the substrate holder was kept at 250 °C during deposition. The deposition time was fixed in 120 min except the biased sample whose duration was incremented in 30 min. Film thicknesses ranged between 350 and 600 nm, except for the non-pulsed DC sample where thickness attained 1500 nm. The coatings were deposited on 316L steel substrates (16–18 wt% Cr, 10–14 wt% Ni, 2–3 wt% Mo) for the mechanical, oxidation and Raman analysis. Their dimensions were 3 cm × 1.5 cm with the following roughness characteristics (Ra = 48 nm, Rq = 61 nm, Rz = 270 nm and Rt = 533 nm). Silicon (100) wafers (thickness 0.525 μm) were used as substrates (1.5 cm × 1.5 cm) for chemical composition, morphological and topological measurements. The substrates were firstly chemically cleaned in ultrasonic baths with acetone and isopropylic alcohol (10 min each) followed by argon etching for 10 min at 500 V inside the chamber.

For plasma characterization, voltage and current waveforms of the pulses applied on the Cr target were measured using a high voltage differential probe (100:1 attenuation) and a PEM Rogowski probe sensor connected to an oscilloscope. The average applied power during the HiPIMS process is defined as the integral of the product of target current I(t), and target voltage, V(t), over the pulse period (T), multiplied by the frequency (f).

$$Average\ power = f \times \int_0^T I(t)V(t)dt$$

The chemical composition of the samples was obtained by electron probe microanalysis (EPMA). The equipment used was a JEOL JXA-8200 SuperProbe instrument equipped with four wavelengths detectors (WDS) and one energy-dispersive X-ray (X-EDS). The observed standard deviation for each concentration is about 1 at.%.

The X-ray diffraction (XRD) patterns were obtained in a X'Pert Pro PANALYTICAL diffractometer in glancing angle (GIXRD) configuration (1°) using Cu Kα (1.54 Å) radiation. The peak position, full width at half maximum (FWHM), and integrated intensity were calculated from the fit of the Bragg reflections using Voigt functions, after background subtraction. The crystal domain sizes and strain contributions were estimated from the Cauchy and Gaussian integral of (111) line profile according to de Keijser et al. [37].

The morphology and thickness of the as-prepared coatings, deposited on silicon substrates, were studied using a high-resolution scanning electron microscope (SEM HITACHI-S4800 equipped with a field emission gun and X-EDS detector (Bruker, XFlash-4010)). Cross-section views were obtained by cleaving the coated silicon substrates.

Root mean square roughness values were determined by means of a stylus profilometer from MAHR using 5.6 mm scanning lengths (3 replica) on the deposited silicon substrates to determine the topographical features strictly connected to the film growth.

Mechanical properties were measured by nanoindentation in an iNano® nanoindenter manufactured by KLA-Tencor using a diamond Berkovich indenter. The equipment, which constantly measures contact load and penetration depth during the semi-static tests, uses the equations described by Oliver and Pharr [38] to determine hardness and elastic modulus at the peak load and the first stages of unloading respectively. However, a small oscillating load was superposed to the load

Table 1
HiPIMS deposition parameters, thickness and chemical composition of the CrN samples.

Sample	Ar flux sccm	N_2 flux sccm	Bias V	Pulse length μs	Frequency Hz	Thickness nm	Cr (EPMA) at. %	N (EPMA) at.%	O (EPMA) at.%	N/Cr
A	20	2	0	20	1000	350 ± 30	49.2 ± 0.5	46.8 ± 0.5	4.0 ± 0.04	0.95
B	20	2	0	40	500	430 ± 20	51.6 ± 0.5	41.8 ± 0.4	6.6 ± 0.1	0.81
C	20	2	0	100	200	450 ± 40	57.6 ± 0.6	38.4 ± 0.4	4.0 ± 0.04	0.67
D	20	4	0	20	1000	400 ± 25	46.5 ± 0.5	50.3 ± 0.5	3.2 ± 0.03	1.08
E	20	4	0	40	500	470 ± 50	49.4 ± 0.5	48.0 ± 0.5	2.6 ± 0.03	0.97
F	20	4	0	100	200	470 ± 30	57.0 ± 0.6	42.0 ± 0.4	1.0 ± 0.02	0.74
Bias	20	4	100	20	1000	580 ± 30	47.7 ± 0.5	52.3 ± 0.5	0.0 ± 0.02	1.10
DC	20	4	0	0	0	1500 ± 50	54.8 ± 0.5	34.3 ± 0.3	10.9 ± 0.1	0.63

function during the loading segment, using the Continuous Stiffness Measurement (CSM) option of this system [39], which allows calculating both properties along the whole loading segment as a function of penetration depth. The measurements were done considering only the region in which the indentation depth did not exceed 10% of the thinnest coating thickness, i.e. 20–35 nm, disregarding lower depths strongly affected by surface roughness. This criterion is widely accepted to ensure the measurements are not affected by the substrate properties [40]. In order to avoid size effects when comparing the results from different coatings, the same indentation depth range was used for all the specimens. The modulus values presented in this paper are the actual coatings Young's modulus, which were calculated from the tip modulus, and the Poisson's ratios of both, tip and coating, according to the equation:

$$\frac{1}{E_r} = \frac{1-\nu_i^2}{E_i} + \frac{1-\nu_c^2}{E_c}$$

where E_r is the reduced modulus experimentally obtained by nanoindentation, E_i and ν_i the Young's modulus and Poisson's ratio of the diamond tip, and ν_c the Poisson's ratio of the coatings, which were obtained from the materials engineering database "MatWeb".

A 4 × 4 nanoindentation array was defined on the surface of each coating, with a 10 μm separation between consecutive indents to avoid effects from previous measurements. The CSM mode used and the number of indents in every sample allowed enough statistical data to obtain reliable and accurate results.

Oxidation of the CrN films was carried out by annealing in air (static) inside a muffle at atmospheric pressure at 600 °C for 2 h and 5 °C/min as heating ramp.

Raman spectra (200–2000 cm^{-1}) were measured using a LabRAM Horiba Jobin Yvon spectrometer equipped with a CCD detector and a diode-pumped solid state laser (532 nm) at 5 mW. All the samples were analyzed during 100 s of exposure time, using an aperture hole of 100 μm.

3. Results

Fig. 1 depicts the measured I-V curves on the cathode for the different HiPIMS discharges at 2 and 4 sccm of nitrogen flow (cf. Fig. 1a and b, respectively). The applied frequencies were fixed at 200, 500 and 1000 Hz, and their corresponding pulse lengths at 100, 40 and 20 μs respectively, so that the duty cycle conditions were identical and constant at 2% for all the deposition processes. At long pulses we found the typical shape of the current pulse characterized by three zones: plasma ignition, decay after reaching maximum current and steady plateau, in close agreement with previous works [1,2,32]. The voltage was found to be constant at 600 V by keeping constant the average sputtering power density at 14.8 W/cm^2 and duty cycle of 2%. A maximum peak intensity of 47 A was obtained for 20 μs and 4 sccm N_2 flow, while the maximum values for the remaining conditions varied slightly between 30 and 35 A. Shorter pulse lengths lead to higher peak intensities, which are associated to higher ionization values as reported by Alami et al. [31] and Konstantinidis et al. [35]. This effect has a consequence on the deposition rate as can be concluded from next figures. Fig. 2a represents the average applied power value for each particular synthesis condition. The deposition rate vs. average power chart (cf. Fig. 2b) shows a linear increment from 2.8 to 3.9 nm/min for the HiPIMS samples, with the lowest values corresponding to the shortest pulses (20 μs). The application of a bias supposed a slight diminution over the linear regression obtained with the rest of the HiPIMS coatings. The deposition rate for the non-pulsed DC specimen, with the same effective average power than sample D (approximately 250 W) but working in constant mode, rose by a factor of four. The average deposition rates normalized to the applied power densities gave a mean value for the HiPIMS samples of 6.4×10^{-4} nm·min^{-1}·W^{-1}·cm^{-2}, which

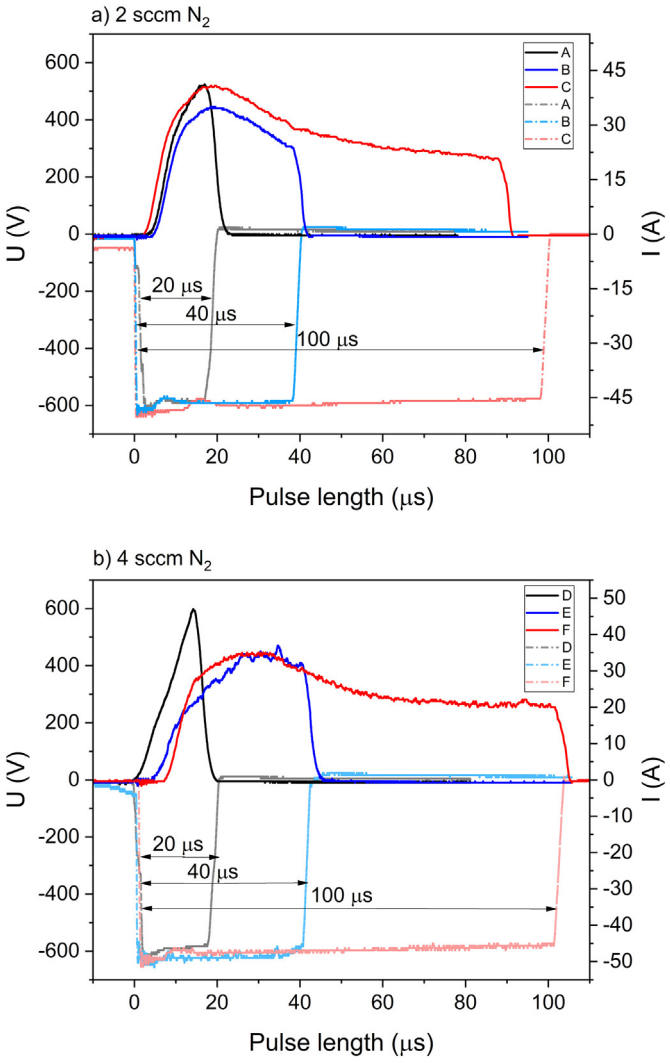

Fig. 1. Intensity (I) and voltage (U) waveforms measured on the cathode for the different HiPIMS discharges at a nitrogen flow of 2 (a) and 4 sccm (b) respectively. The nominal target power is 300 W with a constant duty cycle of 2%.

represented approximate the 25% of the DC deposition rate. The diminution of the deposition rate is well known in HiPIMS [3,28] and relies on the back-attraction of the higher fraction of positive target ions formed during the HiPIMS discharge [32,35]. This effect is particularly significant for materials with subunity sputtering yield [41].

Another remarkable observation is the fact that the modification of the pulse characteristics led to significant variations on the chemical composition without changing the reactive gas mixture. In particular, Fig. 3 shows how the N/Cr ratio goes from slightly over-stoichiometric to sub-stoichiometric CrN by increasing the pulse length. An increased incorporation of nitrogen was also observed previously in CrAlN deposited using short pulses (40 μs) [22]. This finding can be explained by the high concentration of N^+ (main) and N^{2+} ions in the HiPIMS discharge as demonstrated by time and energy resolved ion mass spectroscopic studies [42,43] at the shorter pulses. When reducing the nitrogen flow (2 sccm instead of 4 sccm), further diminution of N/Cr ratio is consequently achieved. Contrarily, the application of a bias had negligible effect on the film composition (1.10 vs. 1.08 in sample D) although can influence the ion energy distribution [43]. This can be explained by the higher N^+ and N_2^+ contents in the HiPIMS discharges and their lower sputtering yield than heavier Ar^+ ions [44]. However, the elimination of HiPIMS pulses to work in DC constant mode modified substantially, both the N/Cr ratio (0.63) and the oxygen contamination

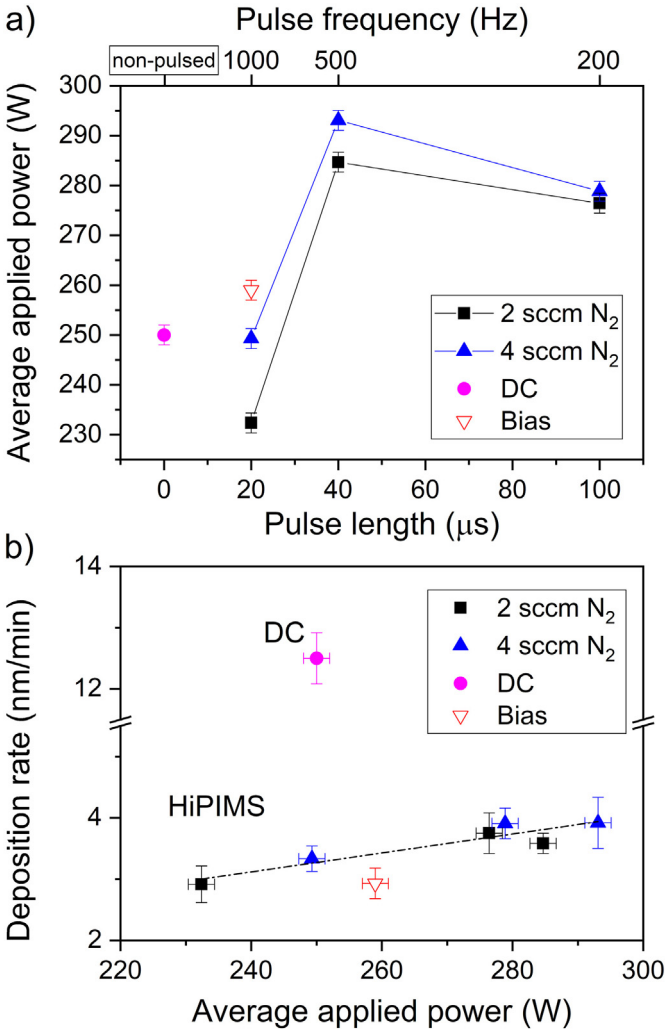

Fig. 2. Average applied power vs. pulse characteristics (a) and variation of the deposition rate vs. average applied power (b) for the CrN films under study.

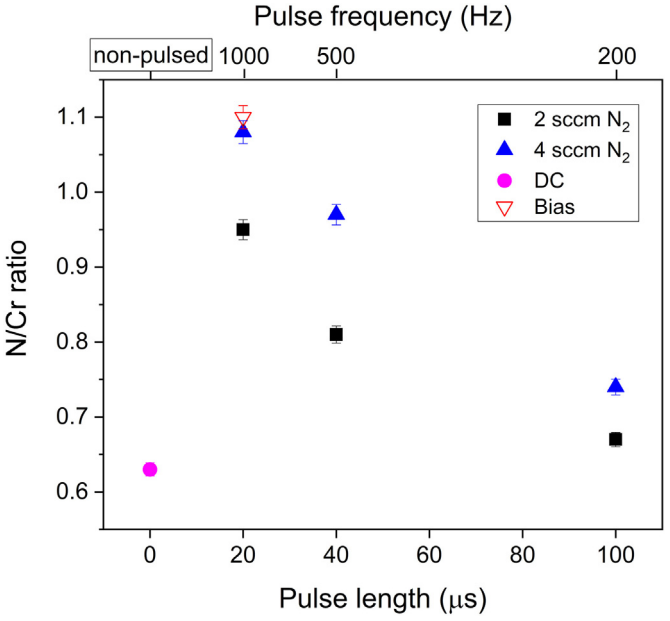

Fig. 3. Measured N/Cr ratios for the set of CrN films depending on the synthesis conditions (pulse length and frequency).

(up to 10 at.%) according to the lower ion density and increased open morphology respectively. Higher N_2/Ar ratios (> 0.45) have been reported to be necessary to obtain stoichiometric CrN phase in standard magnetron sputtering, particularly at low ion bombardment [44,45]. In this case, contrarily to the work of Greczynski et al. [28] where the film stoichiometry was studied at a constant pulse length of 200 μs, HiPIMS has been shown to represent an advantageous tool to obtain stoichiometric CrN with lower nitrogen consumption, as it is less sensitive to target poisoning than DC magnetron sputtering [3]. In addition, a significant incorporation of nitrogen is expected to take place during the high-power pulse due to the high concentration of energetic N^+ and N_2^+ species detected in the plasma [16,41]. Recently, Bakhit et al. showed that stoichiometric TiB_2 films can be obtained by adjusting the length pulses in non-reactive mode (pure Ar discharges) [33]. The selection of pulse waveform in HiPIMS appears thus as an interesting approach to control the film stoichiometry without modification of the reactive gas fluxes. This means an important technical advantage for industrial applications, since changing the reactive gas composition requires certain time until the chamber atmosphere reaches uniformity, and the plasma achieves a steady-state.

For a deeper investigation of the influence of pulse characteristics on the produced film features, crystalline composition and film morphology of the deposited coatings were studied by GIXRD and SEM respectively. Fig. 4 depicts the diffractograms obtained for the entire set of coatings at an incidence angle of 1°. The main diffraction peaks correspond to the cubic CrN carlsbergite phase (PDF 1-76-2494) although differ in the position and width. The coexistence of hexagonal Cr_2N phase (PDF #35-803) is plausible in samples C and non-pulsed DC, attending to the small peak appearing at approximately 67°, corresponding to the (300) reflection. The lowest N/Cr ratios obtained for these two coatings may favor the stability of the hexagonal Cr_2N phase, richer in Cr. The narrowest peaks, with good agreement with the theoretical values for CrN, are obtained at a frequency of 1000 Hz and 4 sccm of N_2 flux (sample D) and non-pulsed DC. However, the use of either lower nitrogen fluxes or lower frequencies (longer pulses), led to a substantial peak widening and shift to higher angles. Conversely, the application of a bias induced a certain degree of left-shifting, probably linked to the introduction of compressive stresses and CrN stoichiometry closer to 1. The peak profile of the (111) reflection was analyzed using the method described in [37] to obtain crystalline structural

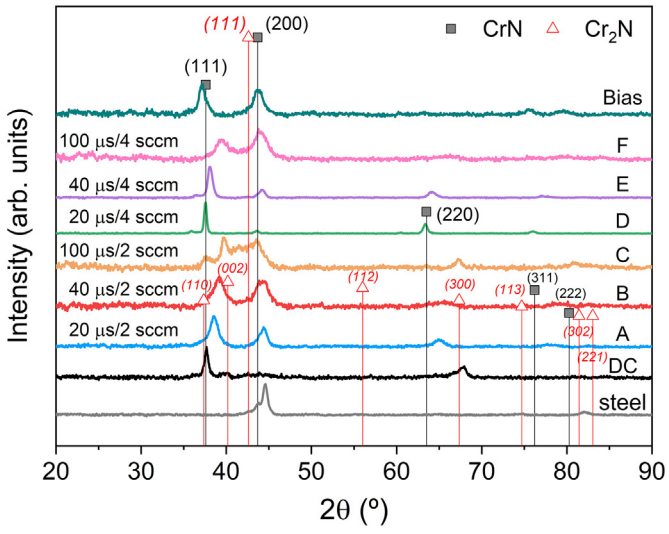

Fig. 4. XRD diffractograms of the CrN films deposited on 316L steel measured in glancing angle configuration (1°). The XRD spectrum of the steel substrate is included as reference. The position of CrN and Cr_2N phases are included (JCPDS card numbers: CrN (PDF #76-2494) and Cr_2N (PDF #35-803)). The reflections with relative intensities higher than 40 are indexed.

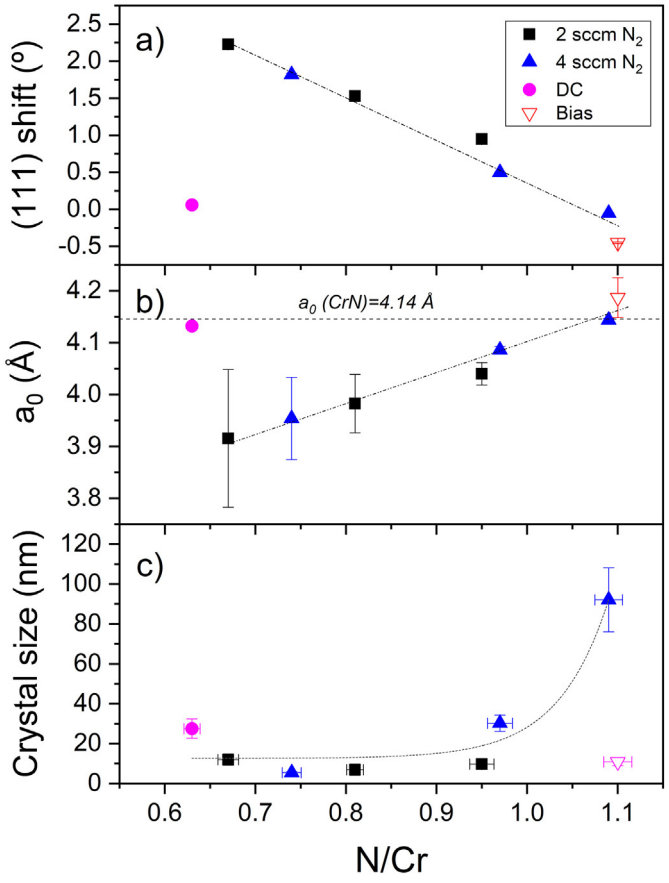

Fig. 5. Crystallographic data obtained from (111) XRD diffraction peak as a function of the N/Cr ratio: peak shift (a), lattice parameter (b) and crystal size (c). The standard deviation values obtained using the (111), (200) and (220) reflection peaks were used as error measures.

information. The dependence of the crystalline features (crystal size, lattice parameter and peak shift using the (111) reflection) on the CrN chemical composition is shown in Fig. 5. The strain values obtained for all the films were found to be below 0.2% indicating the predominance of crystal size effects to peak broadening.

Fig. 5a illustrates the shift of the (111) peak of CrN with respect to the tabulated angle position. A linear dependence on the N/Cr ratio for the HiPIMS samples is clearly observed, with the highest shifts corresponding to the most sub-stoichiometric CrN films. The estimation of the lattice parameter (cf. Fig. 5b) also revealed a correlation with the nitrogen content, approaching the theoretical value of 4.14 Å (cubic CrN-carlsbergite) for N/Cr close to 1.1. An exception is found for the non-pulsed DC specimen (N/Cr = 0.63), whose lattice parameter does not follow the trend, agreeing quite well with the expected values for this phase. This result can be explained by the concomitant presence of the Cr_2N phase, lowering the overall coating N/Cr ratio. In Fig. 5c, the variation of the crystal size vs. N/Cr ratio shows an exponential growth for the HiPIMS layers, reaching the maximum size of ca. 61 nm for sample D, prepared at 4 sccm and 1000 Hz. When this film is repeated using the same pulse parameters and biasing the substrate, the crystal size is significantly reduced because of the additional bombardment of the growing film with energetic ions. Conversely, the use of conventional DC magnetron sputtering without pulses rendered a higher crystal size.

Another interesting conclusion can be inferred from the study of the relative intensities of the diffraction peaks. The decrease of the pulse frequencies (longer duration of pulses) or the application of bias leads to a reduction of the (111) vs. (200) intensity. Development of (111) preferred orientation was observed on polycrystalline CrN coatings grown by magnetron sputtering at moderate ion bombardment [46]. However, coatings composed of grains with (200) and (220) orientations are developed under intense bombardment due to preferential sputtering and collisional dissociation of N_2^+ ions at the film surface. Our results are then consistent with an increase of the ion flux and energy with lower frequencies and bias voltages. The remarkable preferred orientation in the non-pulsed DC sample can be understood by its significant increase in coating thickness, which favors the (111) vs. (200) through competitive growth.

Fig. 6 presents the SEM micrographs obtained in planar and cross-section views for the entire set of samples. In the first six pictures (A to F), the films prepared at 2 sccm of N_2 are shown on the left and those prepared at 4 sccm of N_2 on the right column. The last row depicts the reference samples: non-pulsed DC (left) and Bias (right). The coatings present a typical columnar growth that results more evident in the most crystalline specimens. The bias application clearly influenced the film morphology, disrupting the column growth and densifying the structure. Greczynski et al. [28] reported that columnar growth suppression was achieved for CrN films prepared at N_2/Ar fluxes ≥ 0.3 only if a high bias voltage (150 V) is applied, or when nitrogen contents were below 33 at.% and Cr_2N became the dominant phase. In this work, a suppression of columnar growth is achieved with an average bias of only 100 V and $N_2/Ar = 0.2$. The presence of triangular and pyramidal shapes is clearly evidenced from the SEM top view images of samples A, D and E, which correspond to the coatings with N/Cr > 0.95. The formation of pyramidal column tips is the result of the open columnar structure and the preferred (111) oriented growth, as highlighted previously [5]. The biased sample, whose N/Cr ratio was 1.1, does not exhibit this microstructure because of effective ion bombardment during growth. The microstructure changes from regular faceted to more granular in specimens B and F, attending to a more disordered crystalline structure together with N depletion. Coatings C and non-pulsed DC develop more elongated features (rice-like morphology) that could be influenced by the coexistence of the Cr_2N phase. The root mean square roughness values measured by stylus profilometer were found to be below 10 nm in all specimens, except for the film prepared in constant DC mode, whose roughness increased significantly up to 31 nm. The increase in the total bombarding flux and the fraction of metallic ions in the plasma, have been already pointed to be responsible for the roughness drop and film densification [22,31]. In addition to the lower adatom mobility in DC mode, the larger thickness of this coating compared to those produced by HiPIMS should also be considered. This increased porosity of the surface region leads to a higher interface area for oxidation reaction, which influences the higher oxygen penetration found in this sample.

Fig. 7 depicts the hardness and elastic modulus values obtained for the samples under study for the different pulse conditions. Average hardness values for the pulsed CrN coatings ranged between 6 and 15 GPa. Similar range of values was found by Haye et al. [34] in CrN samples prepared at floating potential. The extreme cases correspond to the specimens prepared in pure DC mode and the biased one, with the lowest (5 GPa) and highest (22.5 GPa) values respectively. The mechanical properties seem to correlate with the pulse characteristics, with higher hardness and Young's moduli for longer pulses. Hsiao et al. found conversely a hardness increase for AlCrN films with increasing frequencies at the duty cycle of 2% (i.e. shorter pulses) [29]. Many different parameters influence the mechanical response (phase composition, crystal size, texture, film morphology, chemical composition, compressive stress, etc.) although some factors may become dominant under certain conditions [18,44]. The average hardness values of CrN_x films with (111)-preferred crystal orientation are typically 12–14 GPa while (200)-texture exhibits nanohardness values of 18 GPa [12,47] and higher (up to 23 GPa) are reported for predominant (200) orientation [5]. In our case, the measured values are in agreement with the reported data for (111) texture and no external biasing of the samples. The sub-stoichiometric CrN_x nature further influences the non-

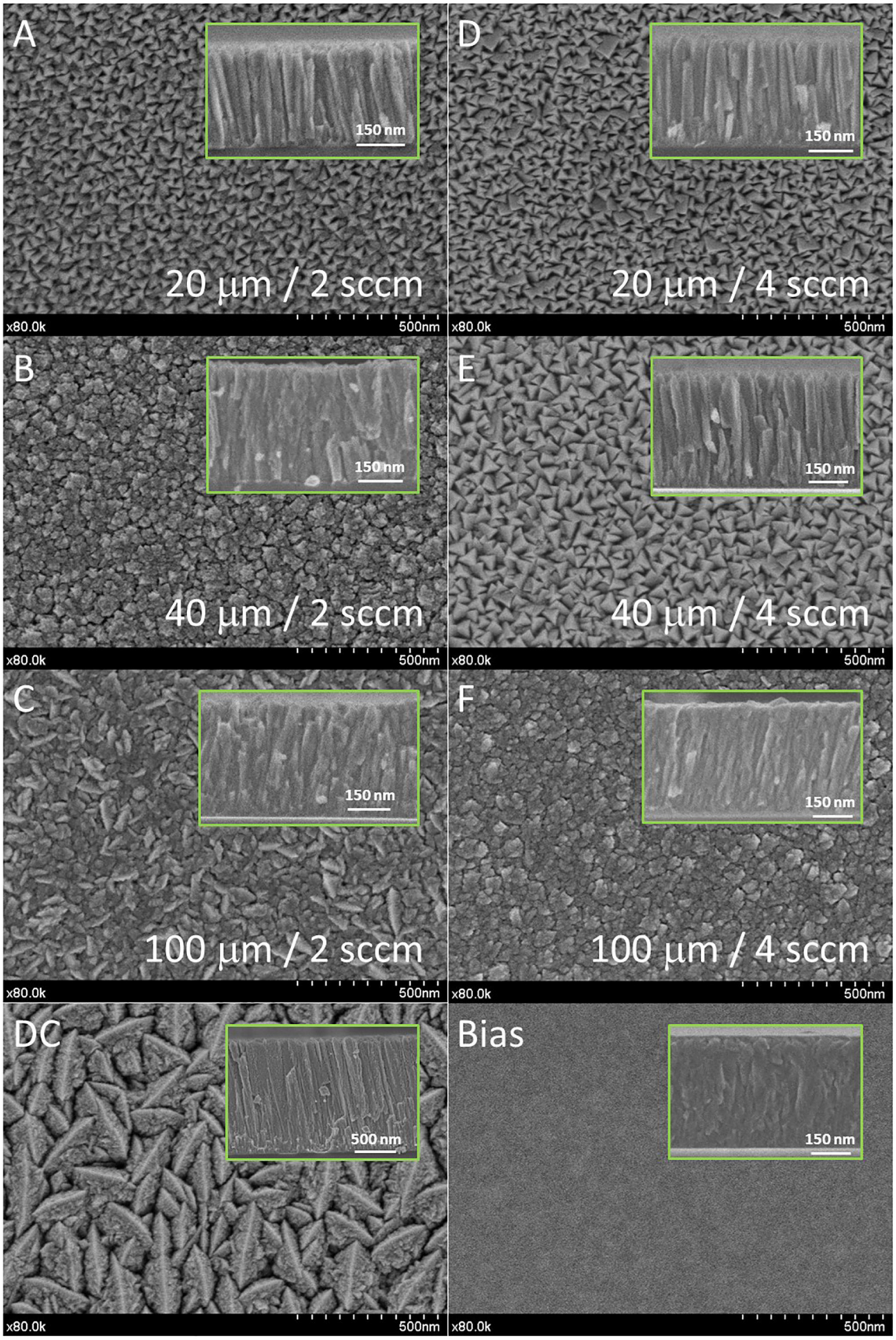

Fig. 6. SEM top and cross-section views of the CrN films under study. The labels refer to the film notation given in Table 1 and were completed with the employed nitrogen flow and pulse duration.

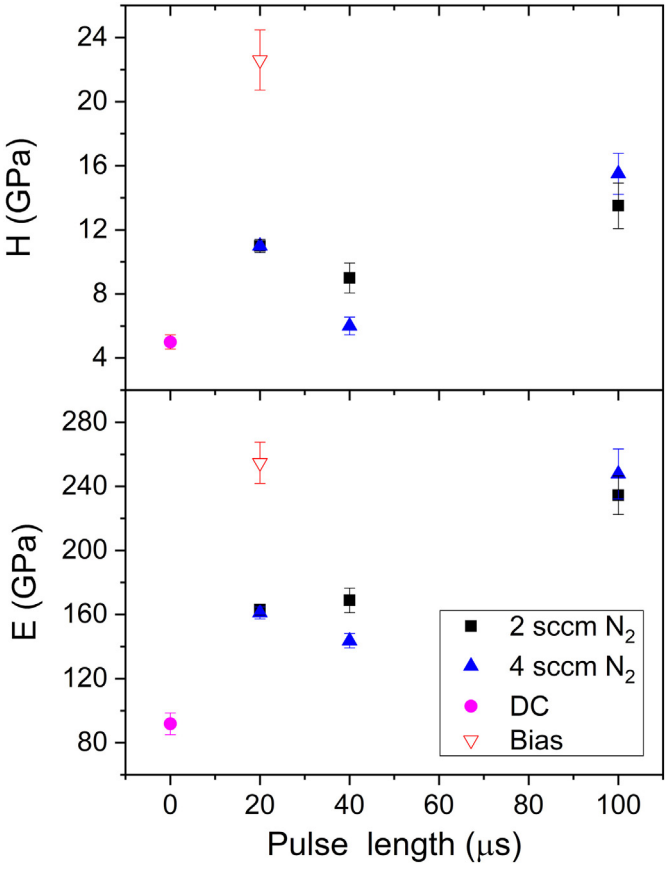

Fig. 7. Mechanical properties depending on the HiPIMS pulse length: hardness (a) and Young modulus (b) values.

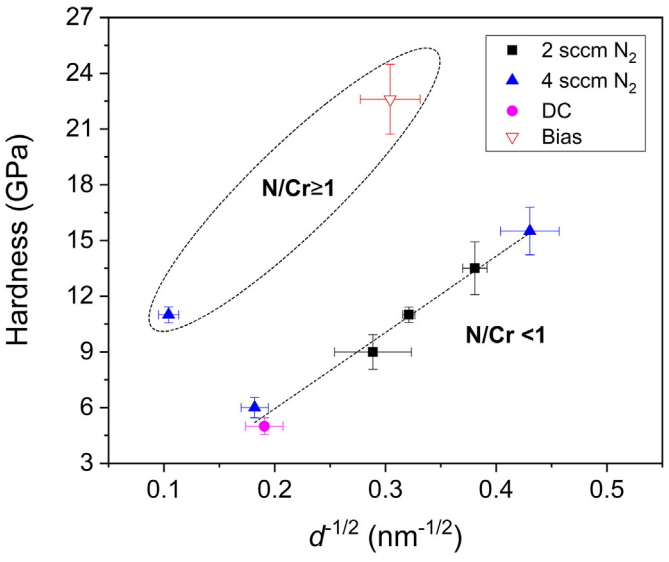

Fig. 8. Hall-Petch dependence of film hardness with crystal size estimated by XRD.

achievement of high hardness values although a clear enhancement is observed by decreasing the CrN crystal size due to the very well-known Hall-Petch effect (see Fig. 8). Smaller grains cause stopping of dislocation motion and thereby strengthen the material. Between the samples with N/Cr ≥ 1, that one with lower crystal size (bias) also reported a hardness enhancement. The benefits of a bias voltage to rise hardness and modulus becomes evident, since increasing the flux and

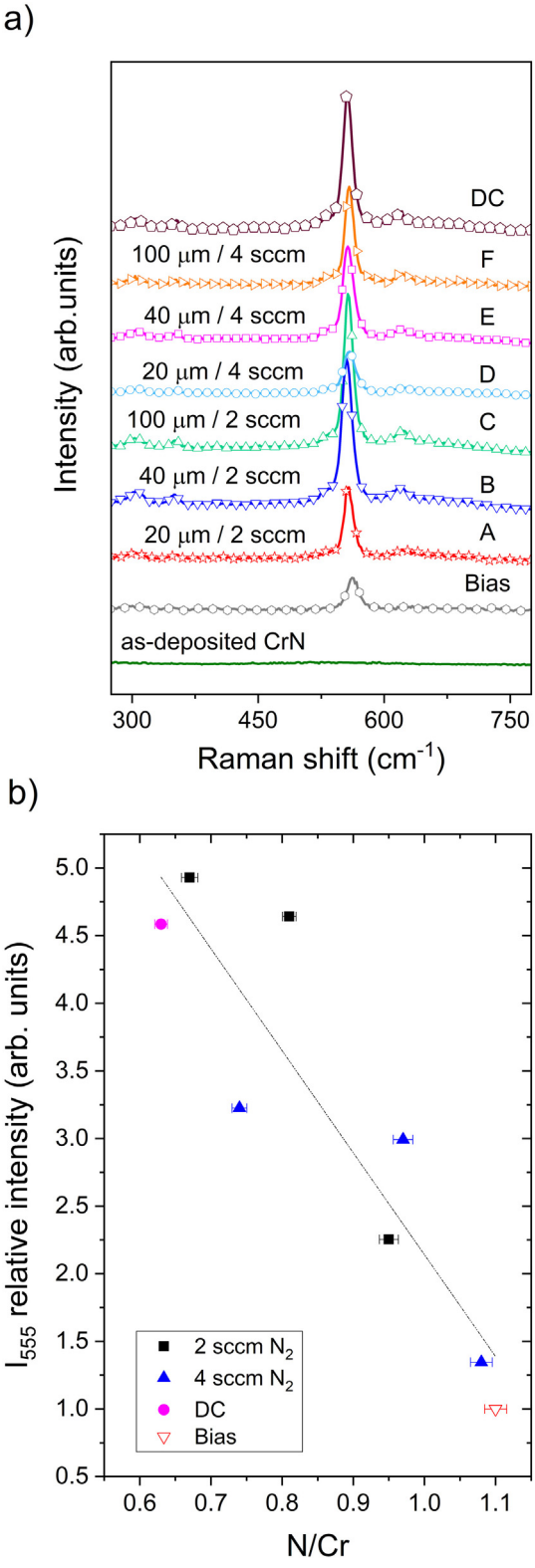

Fig. 9. Raman spectra in the region from 300 to 750 cm^{-1} after annealing at 600 °C/2 h (a) and plot of the I_{555} peak intensity vs. N/Cr ratio (b).

energy of the impinging ions onto the growing film produce denser layer structures and increasing compressive stress, as manifested in its associated XRD diffractogram (cf. Fig. 4).

Fig. 9a shows the Raman spectra obtained for the coatings after annealing at 600 °C in air for 2 h. The spectrum of a non-heated CrN film is included as reference. In all the cases, an intense peak centered

at 555 cm^{-1} is observed, although showing different intensities. This strong band is characteristic of Cr_2O_3 together with the small bands situated at lower frequencies, i.e. 305 and 348 cm^{-1}, which are more visible in the samples displaying higher intensities of the I_{555} peak. The Cr_2O_3 formation on CrN films is widely reported to occur from 500-600 °C due to the outward diffusion of chromium and inward diffusion of oxygen [18,48]. The lowest and highest intensities are obtained for the specimens prepared with bias and pure DC respectively. In the absence of power pulses, the coatings developed a marked open columnar microstructure. Contrarily, higher film compaction is obtained under energetic ion bombardment provided by the target pulsing and the substrate biasing. Fig. 9b presents the relative intensity of the Cr_2O_3 main peak vs. N/Cr ratio, using the biased sample as a reference. We found a clear relationship (the linear fit is plotted as eye-guide) between both variables. We can therefore state that increasing the number of N vacancies in the CrN lattice drives to a decrease of the oxidation resistance [9]. From a structural point of view, the existence of high lattice defects density and vacancies explains the larger oxidation rate because ionic diffusion processes (Cr-outwards and O-inwards) are facilitated. Specimen D is among the HiPIMS layers the one showing the lowest oxidation (excluding the biased one). The synthesis conditions for this coating led to the largest crystal size and N/Cr > 1 (absence of vacancies), favoring structural and thermal stability. Nevertheless, further improvement can be achieved by simultaneous application of a bias during CrN growth. The higher film compaction obtained under the ion bombardment hinders oxygen inward diffusion, and hence, increases the oxidation resistance. Further investigations at different bias voltages will support the validity of the present study.

4. Conclusions

It is possible to produce different film stoichiometries in reactive deposition of CrN films by HiPIMS modifying the pulse characteristics at constant nitrogen flow and duty cycle. Changing the pulse length (or frequency) and operating at duty cycle conditions of 2% allowed modifying the CrN_x stoichiometry from 0.67 to 0.95 and from 0.74 to 1.1 for a constant nitrogen flux of 2 and 4 sccm respectively. These chemical composition variations are accompanied by clear changes in crystallinity, lattice parameter, film morphology and functionality. In this particular case, we have analyzed its influence on the mechanical and oxidation-resistant properties. The best results are obtained with the most intense peak currents, generating more crystalline and stoichiometric CrN films. Further improvement can be obtained by the additional ion bombardment provided by the application of a negative substrate bias (average 100 V). Despite the diminution of the coherent crystal size, the higher film density and compaction favored the increment of hardness and elastic moduli, as well as the oxidation resistance. This tool results very useful to develop different coating architectures and gradient compositions with tailored properties without modification of the reactive gas fluxes, making the transition between layers more feasible.

CRediT authorship contribution statement

J.C. Sánchez-López:Conceptualization, Methodology, Investigation, Writing - original draft, Writing - review & editing, Supervision, Funding acquisition.**A. Caro**:Visualization, Investigation.**G. Alcalá**:Visualization, Investigation, Writing - review & editing.**T.C. Rojas**:Visualization, Investigation, Supervision, Writing - review & editing.

Declaration of competing interest

The authors declare that they have no known competing financial interests or personal relationships that could have appeared to influence the work reported in this paper.

Acknowledgments

European Regional Development Fund program (EU-FEDER) and Spanish Ministry of Economy, Industry and Competitiveness MINECO (projects No. MAT2015-65539-P and MAT2015-69035-REDC, MINECO/FEDER, UE), and CSIC PIE (project 201560E013) are acknowledged for financial support. The authors would like to gratefully acknowledge Mr. Didier Pellerin from ScienTec for performing nanoindentation measurements.

References

[1] A. Anders, Discharge physics of high power impulse magnetron sputtering, Surf. Coat. Technol. 205 (2011) S1–S9.
[2] D. Lundin, K. Sarakinos, An introduction to thin film processing using high-power impulse magnetron sputtering, J. Mater. Res. 27 (2012) 780–792.
[3] K. Sarakinos, J. Alami, S. Konstantinidis, High power pulsed magnetron sputtering: a review on scientific and engineering state of art, Surf. Coat. Technol. 204 (2010) 1661–1684.
[4] A.P. Ehiasarian, J.G. Wen, I. Petrov, Interface microstructure engineering by high power impulse magnetron sputtering for the enhancement of the adhesion, J. Appl. Phys. 101 (2007) 054301.
[5] J. Paulitsch, M. Schenkel, Th. Zufraß, P.H. Mayrhofer, W.-D. Münz, Structure and properties of high power impulse magnetron sputtering and DC magnetron sputtering CrN and TiN films deposited in an industrial scale unit, Thin Solid Films 518 (2010) 5558–5564.
[6] N. Bagcivan, K. Bobzin, G. Grundmeier, M. Wiesingm, O. Ozcan, C. Kunze, R.H. Brugnara, Influence of HPPMS pulse length and inert gas mixture on the properties of (Cr,Al)N coatings, Thin Solid Films 549 (2013) 192–198.
[7] W.D. Münz, D.B. Lewis, P.E. Hovsepian, C. Schönjahn, A. Ehiasarian, I.J. Smith, Industrial scale manufactured superlattice hard PVD coatings, Surf. Eng. 17 (2001) 15–27.
[8] S. Veprek, M.J.G. Veprek-Heijman, Industrial applications of superhard nanocomposite coatings, Surf. Coat. Technol. 202 (2008) 5063–5073.
[9] M. to Baben, M. Hans, D. Primetzhofer, S. Evertz, H. Ruess, J.M. Schneider, Unprecedented thermal stability of inherently metastable titanium aluminum nitride by point defect engineering, Mater. Res. Lett. 5 (2017) 158–169.
[10] M. Stueber, H. Holleck, H. Leiste, K. Seemann, S. Ulrich, C. Ziebert, Concepts for the design of advanced nanoscale PVD multilayer protective thin films, J. Alloys Compd. 483 (2009) 321–333.
[11] L. Hultman, Thermal stability of nitride thin films, Vacuum 57 (2000) 1–30.
[12] E. Martinez, R. Sanjinés, O. Banakh, F. Lévy, Electrical, optical and mechanical properties of sputtered CrN_y films and Cr_{1-x} $Si_xN_{1.02}$ thin films, Thin Solid Films 447-448 (2004) 332–336.
[13] C. Hu, K. Guo, Y. Li, Z. Gu, J. Quan, S. Zhang, W. Zheng, Optical coatings of durability based on transition metal nitrides, Thin Solid Films 688 (2019) 137339.
[14] A.A. Voevodin, M.A. Capano, S.J.P. Laube, M.S. Donley, J.S. Zabinski, Design of a Ti/TiC/DLC functionally gradient coating based on studies of structural transitions in Ti-C thin films, Thin Solid Films 298 (1997) 107–115.
[15] J.A. Santiago, I. Fernández-Martínez, A. Wennberg, J.M. Molina-Aldareguia, M. Castillo, T.C. Rojas, J.C. Sánchez-López, M.U. González, J.M. García-Martín, H. Li, V. Bellido-González, M.A. Monclús, R. González-Arrabal, Adhesion enhancement of DLC hard coatings by HiPIMS metal ion etching pretreatment, Surf. Coat. Technol. 349 (2018) 787–796.
[16] A.P. Ehiasarian, W.-D. Münz, L. Hultman, U. Helmersson, I. Petrov, High power pulsed magnetron sputtered CrN_x films, Surf. Coat. Technol. 163-164 (2003) 267–272.
[17] O. Banakh, P.E. Schmid, R. Sanjines, E. Levy, High-temperature oxidation resistance of $Cr_{1-x}Al_xN$ thin films deposited by reactive magnetron sputtering, Surf. Coat. Technol. 163 (2003) 57–61.
[18] J.C. Sánchez-López, D. Martínez-Martínez, C. López-Cartes, A. Fernández, M. Brizuela, A. García-Luis, J.I. Oñate, Mechanical behavior and oxidation resistance of Cr(Al)N coatings, J. Vac. Sci. Technol. A 23 (2005) 681–686.
[19] L. Wang, X. Nie, J. Houseden, E. Spain, J.C. Jiang, E.I. Meletis, A. Leyland, A. Matthews, Material transfer phenomena and failure mechanisms of a nanostructured Cr-Al-N coating in laboratory wear test and an industrial punch tool application, Surf. Coat. Technol. 203 (2008) 816–821.
[20] J. Lin, B. Mishra, J.J. Moore, W.D. Sproul, A study of the oxidation behavior of CrN and CrAlN thin films in air using DSC and TGA analyses, Surf. Coat. Technol. 202 (2008) 3272–3283.
[21] M.W. Kim, K.H. Kim, M.C. Kang, S.H. Cho, K.T. Ryu, Mechanical properties and cutting performance of Cr-Al-N hybrid coated micro-tool for micro high-speed machining of flexible fine die, Curr. Appl. Phys. 12 (2012) S14–S18.
[22] C. Kunze, R.H. Brugnara, N. Bagcivan, K. Bobzin, G. Grundmeier, Surface chemistry of PVD (Cr,Al)N coatings deposited by means of direct current and high power pulsed magnetron sputtering, Surf. Interface Anal. 45 (2013) 1884–1892.
[23] S. Mato, G. Alcalá, M. Brizuela, R. Escobar Galindo, F.J. Pérez, J.C. Sánchez-López, Long-term high temperature oxidation of CrAl(Y)N coatings in steam atmosphere, Corr. Sci. 80 (2014) 453–460.

[24] T.C. Rojas, S. Domínguez-Meister, M. Brizuela, J.C. Sánchez-López, High-temperature oxidation of CrAlYN coatings: implications of the presence of Y and type of steel, Surf. Coat. Technol. 354 (2018) 203–213.
[25] A.E. Reiter, V.H. Derflinger, B. Hanselmann, T. Bachmann, B. Sartory, Investigation of the properties of $Al_{1-x}Cr_xN$ coatings prepared by cathodic arc evaporation, Surf. Coat. Technol. (7) (2005) 2114–2122.
[26] J.M. Lackner, W. Waldhauser, R. Berghauser, R. Ebner, G. Kothleiner, Growth phenomena in room temperature pulsed laser deposition chromium and chromium nitride coatings, Surf. Coat. Technol. 200 (2005) 387–390.
[27] J. Lin, J.J. Moore, W.D. Sproul, B. Mishra, Z. Wu, J. Wang, The structure and properties of chromium nitride coatings deposited using dc, pulsed dc and modulated pulse power magnetron sputtering, Surf. Coat. Technol. 204 (2010) 2230–2239.
[28] G. Greczynski, J. Jensen, J. Böhlmark, L. Hultman, Microstructure control of CrN_x films during high power impulse magnetron sputtering, Surf. Coat. Technol. 205 (2010) 118–130.
[29] Y. Hsiao, J. Lee, Y. Yang, B. Lou, Effects of duty cycle and pulse frequency on the fabrication of AlCrN thin films deposited by high power impulse magnetron sputtering, Thin Solid Films 549 (2013) 281–291.
[30] K. Bobzin, T. Brögelmann, R.H. Brugnara, Aluminum-rich HPPMS $(Cr_{1-x}Al_x)N$ coatings deposited with different target compositions and at various pulse lengths, Vacuum 122 (2015) 201–207.
[31] J. Alami, K. Sarakinos, F. Uslu, M. Wuttig, On the relationship between the peak target current and the morphology of chromium nitride thin films deposited by reactive high power pulsed magnetron sputtering, J. Phys. D. Appl. Phys. 42 (2009) 015304.
[32] A. Ferrec, J. Kéraudy, P.Y. Jouan, Mass spectrometry analyzes to highlight differences between short and long HiPIMS discharges, Appl. Surf. Sci. 390 (2016) 497–505.
[33] B. Bakhit, I. Petrov, J.E. Greene, L. Hutman, J. Rosén, G. Greczynski, Controlling the B/Ti ratio of TiB_x thin films grown by high-power impulse magnetron sputtering, J. Vac. Sci. Technol. A 36 (2018) 030604.
[34] E. Haye, J.L. Colaux, P. Moskovkin, J.J. Pireaux, S. Lucas, Wide range investigation of duty cycle and frequency effects on bipolar magnetron sputtering of chromium nitride, Surf. Coat. Technol. 350 (2018) 84–94.
[35] S. Konstantinidis, J.P. Dauchot, M. Ganciu, A. Ricard, M. Hecq, Influence of pulse duration on the plasma characteristics in high-power pulsed magnetron discharges, J. Appl. Phys. 99 (2006) 013307.
[36] J. Alami, K. Sarakinos, G. Mark, M. Wuttig, On the deposition rate in a high power pulsed magnetron sputtering discharge, Appl. Phys. Lett. 89 (2006) 154104.
[37] Th.H. de Keijser, J.I. Langford, E.J. Mittemeijer, A.B.P. Vogels, Use of Voigt function in a single-line method for the analysis of X-ray diffraction line broadening, J. Appl. Crystallogr. 15 (1982) 308–314.
[38] W.C. Oliver, G.M. Pharr, An improved technique for determining hardness and elastic-modulus using load and displacement sensing indentation experiments, J. Mater. Res. 7 (1992) 1564–1583.
[39] J.L. Hay, P. Agee, E.G. Herbert, Continuous stiffness measurement during instrumented indentation testing, Exp. Tech. 34 (2010) 86–94.
[40] G. Alcalá, S. Mato, P. Skeldon, G.E. Thompson, A.B. Mann, H. Habazaki, K. Shimizu, Mechanical properties of barrier-type anodic alumina films using nanoindentation, Surf. Coat. Technol. 173 (2003) 293–298.
[41] D.J. Christie, Target material pathways model for high power pulsed magnetron sputtering, J. Vac. Sci. Technol. A 23 (2005) 330–335.
[42] C. Greczynski, L. Hultman, Time and energy resolved ion mass spectroscopy studies of the ion flux during high power pulsed magnetron sputtering of Cr in Ar and Ar/N_2 mixtures, Vacuum 84 (2010) 1159–1170.
[43] K. Bobzin, T. Brögelmann, R.H. Brugnara, N.C. Kruppe, S. Chromy, Influence of HPPMS pulse parameters on the reactive gas N_2 and on the properties of (Cr,Al)N coatings, Surf. Coat. Technol. 293 (2016) 28–34.
[44] T. Hurkmans, D.B. Lewis, H. Paritong, J.S. Brooks, W.D. Münz, Influence of ion bombardment on structure and properties of unbalanced magnetron grown CrN_x coatings, Surf. Coat. Technol. 114 (1999) 52–59.
[45] P.H. Mayrhofer, G. Tischler, C. Mitterer, Microstructure and mechanical/thermal properties of Cr-N coatings deposited by reactive unbalanced magnetron sputtering, Surf. Coat. Technol. 142-144 (2001) 78–84.
[46] R. Daniel, K.J. Martinschitz, J. Keckes, C. Mitterer, Texture development in polycrystalline CrN coatings: the role of growth conditions and a Cr interlayer, J. Phys. D. Appl. Phys. 42 (2009) 075401.
[47] P. Hones, M. Diserens, R. Sanjinés, F. Levy, Electronic structure and mechanical properties of hard coatings from the chromium–tungsten nitride system, J. Vac. Sci. Technol. B 18 (2000) 2851.
[48] J. Lin, N. Zhang, W.D. Sproul, J.J. Moore, A comparison of the oxidation behavior of CrN films deposited using continuous dc, pulsed dc and modulated pulsed power magnetron sputtering, Surf. Coat. Technol. 206 (2012) 3283–3290.